

Arbitrary Manipulation of Light Intensity by Bilayer Aluminum Metasurfaces

Zhancheng Li, Wenwei Liu, Hua Cheng, Duk-Yong Choi, Shuqi Chen,* and Jianguo Tian

Realizing the arbitrary manipulation of light intensity on the microscale is a fundamental requirement for the miniaturization and integration of optical devices, which would have a substantial impact in the fields of high-resolution imaging and information encryption. Metasurfaces, which have unprecedented capabilities for light manipulation, provide an alternative way to achieve this requirement. Here, alignment-free bilayer metasurfaces composed of aluminum nanorods are utilized to realize full and broadband polarization-selective transmission of optical waves in the near-infrared band. By independently adjusting the orientation angle of each nanorod, it is demonstrated that the proposed design is an appealing alternative for realizing arbitrary intensity manipulation of linearly polarized light; further, it is experimentally validated that the proposed bilayer metasurfaces can be widely used for microscale modulation of light intensity, gray imaging with high resolution, optical polarization encoding, and anti-counterfeiting. The proposed bilayer metasurfaces pave the way for implementing the arbitrary manipulation of light intensity on the microscale.

encryption, plays an invaluable role in modern nanophotonics.^[1–4] Recently, metasurfaces composed of planar sub-wavelength artificial nanostructures have shown great precision and exceptional capabilities for light intensity manipulation. Metasurfaces for frequency-selective transmission, reflection, and perfect absorption have been widely proposed over the past few years, have shown great advantages, and have had a strong impact in the field of optical filters.^[5–10] Currently, the intensity of the transmitted or reflected light can be directly manipulated on the microscale by utilizing the anisotropic optical resonance of nanostructures, which largely improves the application of metasurfaces in polarization-encoded imaging and anti-counterfeiting.^[11–15] However, due to the weak interactions between light and the metasurfaces, full and broadband

Controlling the spatial distribution of light intensity on the microscale, which can be widely used in optical imaging and

manipulation of light intensity on the microscale with a high manipulation depth has yet to be reported.


Dr. Z. Li, Dr. W. Liu, Prof. H. Cheng, Prof. S. Chen, Prof. J. Tian
The Key Laboratory of Weak Light Nonlinear Photonics
Ministry of Education
School of Physics and TEDA Institute of Applied Physics
Nankai University
Tianjin 300071, China
E-mail: schen@nankai.edu.cn

Prof. D.-Y. Choi
Laser Physics Centre
Research School of Physics and Engineering
Australian National University
Canberra, ACT 2601, Australia

Prof. D.-Y. Choi
College of Information Science and Technology
Jinan University
Guangzhou 510632, China

Prof. S. Chen
The Collaborative Innovation Center of Extreme Optics
Shanxi University
Taiyuan, Shanxi 030006, China

Prof. S. Chen
Renewable Energy Conversion and Storage Center
Nankai University
Tianjin 300071, China

 The ORCID identification number(s) for the author(s) of this article can be found under <https://doi.org/10.1002/adom.201900260>.

Recent advances in few-layer metasurfaces have shown some advantages for meeting this challenge. The resonance coupling effect and the optical wave interference effect in few-layer metasurfaces can significantly enhance the interaction between light and nanostructures, which results in an improvement in the working efficiency and controllability of light manipulation.^[16] Compared with metasurfaces, recent approaches have proven that few-layer metasurfaces provide more freedom for manipulating light in both single and multiple dimensions, leading to many new optical functionalities and phenomena.^[17–24] Due to the rapid development of few-layer metasurfaces, they have attracted wide interest among the scientific community for broadband manipulation of light intensity.^[25–29] Huang et al. proposed bilayer metasurfaces to enable dual and broadband antireflection in the terahertz and mid-infrared spectral ranges.^[27] Hu et al. utilized bilayer metasurfaces to demonstrate broadband optical band-rejection filters in the near-infrared spectral range.^[28] Most of these works focused on controlling the reflected light intensity. Full and broadband intensity manipulation of transmitted light has yet to be reported. Moreover, few-layer metasurfaces for full and broadband manipulation of the spatial distribution of light intensity are also desirable and need to be further validated by theoretical analysis and experimental measurements.

Here, we provide an effective approach to realize full and broadband transmission intensity manipulation of linearly

DOI: 10.1002/adom.201900260

polarized light in the near-infrared band by utilizing bilayer metasurfaces composed of aluminum (Al) nanorods. By combining the anisotropic resonance of the nanorods with the optical wave interference in the two layers, broadband polarization-selective transmission can be achieved. The proposed bilayer metasurfaces can be treated as a broadband linear polarizer in the near-infrared band. The simulation results show that the manipulation depth of the polarization-selective transmission in the proposed bilayer metasurfaces is greater than 98% from 1050 to 1350 nm with a working efficiency of greater than 90%, which has been validated by the experimental results. By utilizing the proposed design, the transmission intensity of linearly polarized light can be fully manipulated by simply changing the orientation angle of the nanorods. Further, we experimentally validate that the proposed bilayer metasurfaces can be used for microscale modulation of light intensity, gray imaging with high resolution, optical polarization encoding, and anti-counterfeiting.

A schematic of the designed periodic bilayer metasurface is shown in **Figure 1**. The proposed bilayer metasurface, which is prepared on a SiO₂ substrate, consists of two layers of aluminum nanorods that are embedded in an SU-8 polymer. The nanorods are located at the centers of the hexagonal unit cell ($a_1 = a_2 = 230\sqrt{3}\text{nm}$). The length, width, and thickness of the nanorods are $L = 270\text{ nm}$, $w = 80\text{ nm}$, and $t = 30\text{ nm}$, respectively. The distance between the two layers of nanorods and the thickness of the SU-8 polymer coating the upper layer of nanorods are both equal to 100 nm. The anisotropic resonance of the aluminum nanorods can be enhanced by the optical wave interference between the two layers, resulting in broadband polarization-selective transmission. For linearly polarized incident light with a polarization angle equal to α (the angle between the polarization direction of incident light and the x -axis), the intensity of the transmitted light can be expressed as

$I = A\sin^2\alpha$, where A is the transmission intensity for α equal to 90°. The inset in **Figure 1** shows a scanning electron microscopy (SEM) image of the top view of the fabricated periodic bilayer metasurface that was taken after the experimental measurements. To clearly observe the aluminum nanorods in the upper layer, the SU-8 polymer with thickness approximately equal to 150 nm was etched by oxygen plasma. Then, a very thin layer of platinum was coated onto the surface of the sample. However, due to the small atomic contrast between the Al nanorods and SU-8 polymer and the smooth sample morphology, the aluminum nanorods in the bottom layer could not be observed in the SEM image. The white dots in the SEM image come from the etching residue of the SU-8 polymer. To analyze the optical response of the proposed periodic bilayer metasurface, numerical simulations were conducted using finite differential time domain methods. The optical constants of aluminum were taken from Palik's handbook.^[30] The refractive index of the SiO₂ substrate was taken as 1.51, while the refractive index of the SU-8 polymer was taken as 1.48.

First, we simulated the transmission coefficients of the Jones matrix \mathbf{T} of the proposed bilayer metasurface.^[18] **Figure 2a** shows the simulated results of the modular square $t_{ij} = |T_{ij}|^2$ of the transmission coefficients. The simulated results indicate that the proposed bilayer metasurface can be treated as a linear polarizer for wavelengths from 1050 to 1350 nm with a working efficiency of greater than 90%, whose \mathbf{T} matrix can be expressed as

$$\mathbf{T} = \begin{pmatrix} 0 & 0 \\ 0 & T_{yy} \end{pmatrix} \quad (1)$$

This indicates that the transmission axis of the proposed bilayer metasurface is perpendicular to the long axis of the nanorods. Further simulation analysis indicates that incident

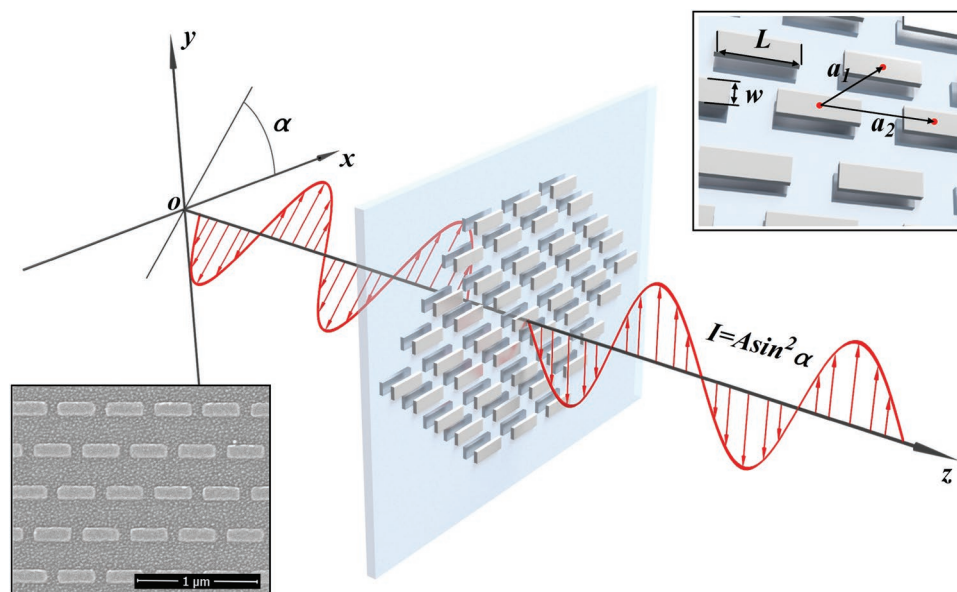


Figure 1. A schematic of the polarization-selective transmission in the designed periodic bilayer metasurface. The transmittance can be expressed as a function of the polarization direction of the linearly polarized incident light over a broad bandwidth. Insets: SEM image of the fabricated periodic bilayer metasurface (bottom left) and a schematic of the designed bilayer metasurface (top right).

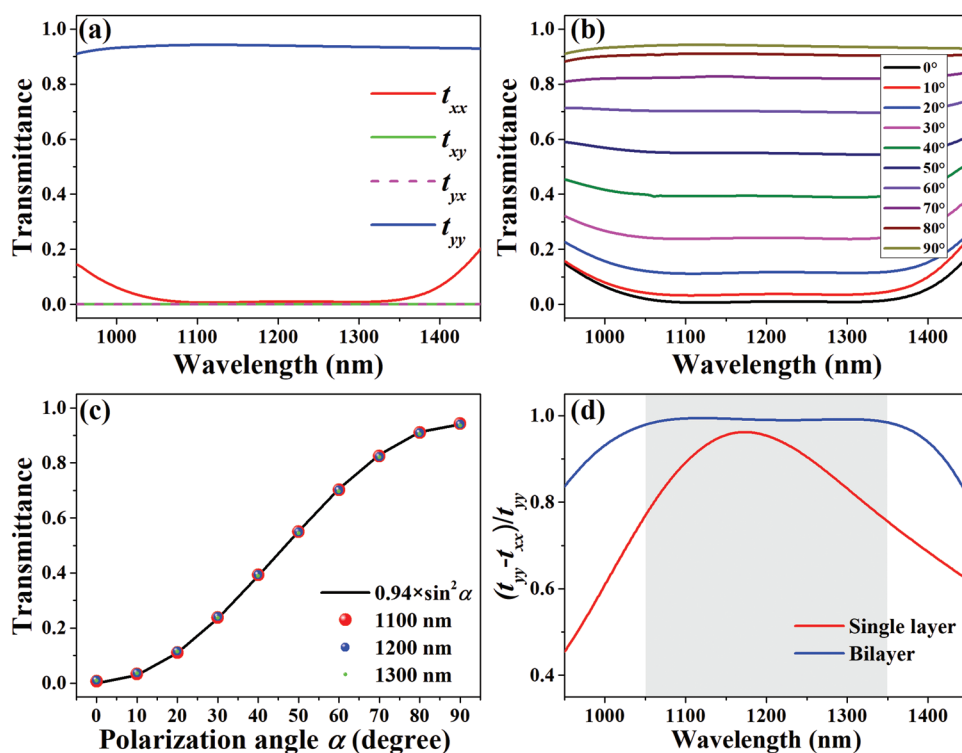


Figure 2. The simulated results for the polarization-selective transmission of the designed bilayer metasurface in which the long axis of the nanorods is along the x -axis. a) The simulated results of the modular square $t_{ij} = |T_{ij}|^2$ of the transmission coefficients of the bilayer metasurface. b) The simulated results of the transmittances under linearly polarized illumination with different polarization angles. c) The transmittances as a function of polarization angle α of linearly polarized incident light at 1100, 1200, and 1300 nm. The line denotes the $I \propto \sin^2 \alpha$ dependence. d) Comparison of the transmission ratio $(t_{yy} - t_{xx})/t_{yy}$ between metasurfaces with a single layer and a bilayer of the nanorods. The shaded region denotes the wavelengths with a transmission ratio greater than 98% for the bilayer metasurface.

waves with a polarization direction along the long axis of the nanorods are mainly reflected and partly absorbed by the designed bilayer metasurface. For linearly polarized incident light with a polarization angle equal to α , the Jones vector \mathbf{J} can be expressed as

$$\mathbf{J}_{\text{in}} = \begin{pmatrix} \cos \alpha \\ \sin \alpha \end{pmatrix} \quad (2)$$

Then, we can obtain the Jones vector of the transmitted light

$$\mathbf{J}_t = \mathbf{T} \mathbf{J}_{\text{in}} = \begin{pmatrix} 0 & 0 \\ 0 & T_{yy} \end{pmatrix} \begin{pmatrix} \cos \alpha \\ \sin \alpha \end{pmatrix} = \begin{pmatrix} 0 \\ T_{yy} \sin \alpha \end{pmatrix} \quad (3)$$

The total intensity of the transmitted light can then be determined by

$$I = A \sin^2 \alpha \quad (4)$$

where $A = |T_{yy}|^2$ is the transmittance when the polarization angle α of the linearly polarized incident light is equal to 90° . Equation (4) reveals the polarization-selective transmission of the proposed periodic bilayer metasurface. Figure 2b shows the simulated transmission spectra under linearly polarized illumination with different polarization angles, which further validates the broadband and full intensity manipulation of the

transmitted light in the proposed periodic bilayer metasurface. To visually describe the relationship between the polarization angle of the incident light and the intensity of the transmitted light, the transmittance as a function of the polarization angle α at 1100, 1200, and 1300 nm is shown in Figure 2c. The results indicate the good consistency between the simulated results and the calculated results at different incident wavelengths. To show the advantages of the bilayer design for light intensity manipulation by utilizing polarization-selective transmission, we compare the transmission ratio (defined as $(t_{yy} - t_{xx})/t_{yy}$) between metasurfaces composed of a single layer of nanorods and bilayer nanorods in Figure 2d. The transmission ratio is greater than 98% for wavelengths from 1050 to 1350 nm for the proposed periodic bilayer metasurface. This result indicates that the transmission ratio is significantly improved over a broad bandwidth by utilizing the bilayer design. The broadband enhancement of the polarization-selective transmission in the proposed bilayer design is mainly attributed to the interference between the multiple reflections and the direct reflection (see Figure S1 in the Supporting Information). From the simulated results (see Figure S2 in the Supporting Information), we further validate that the optical functionality of the proposed bilayer metasurface remains constant when the incident angle of the illumination is no more than 50° . The simulation results also indicate that the optical functionality of the proposed bilayer metasurface has a low requirement regarding the alignment of the nanorods in the two layers

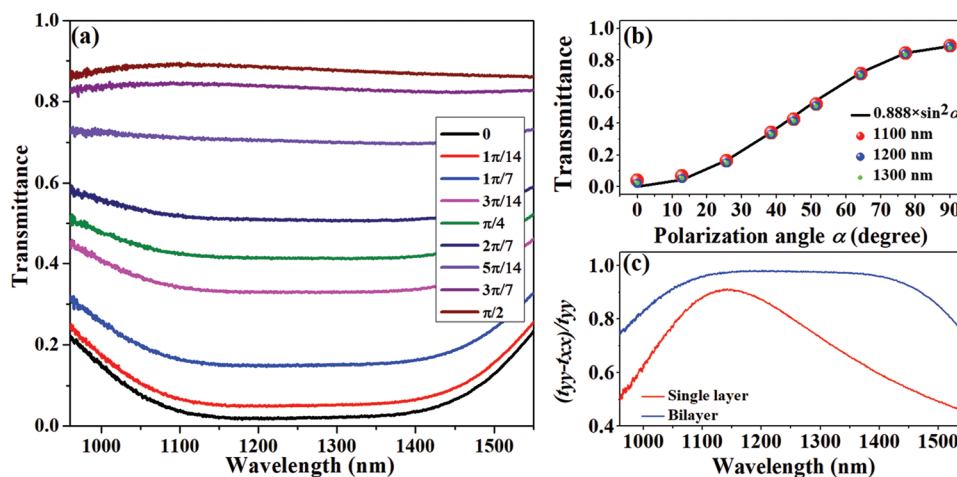


Figure 3. Experimental verification of the polarization-selective transmission of the designed bilayer metasurface. a) The experimental results of the transmittance under linearly polarized illumination with different polarization angles. b) The transmittance as a function of the polarization angle α of the linearly polarized incident light at 1100, 1200, and 1300 nm. The line denotes the $I \propto \sin^2 \alpha$ dependence. c) Comparison of the transmission ratio $(t_{yy} - t_{xx}) / t_{yy}$ between metasurfaces with a single layer and a bilayer of the nanorods.

(see Figure S3 in the Supporting Information). These results prove that the proposed bilayer metasurface can be utilized to realize full intensity manipulation of the transmitted light with the advantages of a compact design, a simple unit structure, having low cost, being alignment free, having a broadband and wide-angle optical response.

Experimental verification of the polarization-selective transmission in the designed bilayer metasurface is shown in **Figure 3**, which is in good agreement with the simulated and calculated results. The transmission spectra were measured by using a Fourier transform infrared spectrometer (VERTEX 70). It is worth mentioning that the polarizer that is used for controlling the polarization state of the incident light in the experiment is integrated in a gear system with a stepwise rotation of $\pi/28$. **Figure 3a** shows the experimental results of the transmittance under linearly polarized illumination at different polarization angles. The 50 nm redshift in the experimental results can be ascribed to minute structural differences between the designed bilayer metasurface and the fabricated one, which is due to the fabrication error. The experimental results of the transmittance as a function of the polarization angle α of the linearly polarized incident light at 1100, 1200, and 1300 nm are shown in **Figure 3b** and are in good agreement with Equation (4) and the simulation results in **Figure 2c**. The significant improvement of the transmission ratio by utilizing the bilayer design is also validated by the experimental results shown in **Figure 3c** (and **Figure S4** in the Supporting Information). The minute shift in the transmission spectra is also attributed to the fabrication tolerances. The good agreement between the experimental results and the simulated results is mainly attributed to the alignment-free design and wide-angle optical response of the bilayer metasurface, which significantly reduces the challenges of the fabrication and measurement processes. We believe that the proposed bilayer metasurface provides an effective means for commercializing few-layer metasurfaces for light intensity manipulation and indicates a promising development for the design and fabrication of few-layer metasurfaces on a larger scale.

Furthermore, according to Equation (4), the transmission intensity is a function of the polarization angle for linearly polarized incident light. Thus, we can change the polarization angle of the incident light to realize intensity manipulation of the transmitted light. Because the proposed bilayer metasurface is designed with a hexagonal unit cell, changing the polarization angle α of the incident light is equivalent to changing the orientation angle θ (angle between the long axis of the nanorods and the x -axis) of the nanorods. Thus, for linearly polarized incident light with a fixed polarization angle, the intensity of the transmitted light can be manipulated by changing the orientation angle θ of the nanorods. This indicates that the proposed bilayer metasurface can be utilized to realize manipulation of the spatial distribution of the transmission intensity by independently designing the orientation angle of the nanorods in each unit cell. To validate this concept, we further propose the application of the proposed bilayer metasurface in the areas of microscale modulation of light intensity, gray imaging with high resolution, optical polarization encoding, and anti-counterfeiting.

First, we designed a gradient optical intensity filter based on the proposed bilayer metasurface by introducing a gradient to the orientation angles of the nanorods along the x -axis. A schematic of the designed intensity filter is shown in **Figure 4a**. The designed intensity filter has ten separate areas in which the square of the sine value of the orientation angle $\sin^2 \theta$ varies from 0 to 0.9 along the x -axis at a stepwise rate of 0.1. According to Equation (4), for x -polarized incident light, the transmission intensity in the proposed intensity filter will vary from 0 to 0.9A along the x -axis at a stepwise rate of 0.1A. **Figure 4b** shows the experimental results for the spatial distribution of the transmission intensity at 1200 nm, which is in good agreement with the calculated distribution in **Figure 4a**. This result validates that the proposed bilayer metasurface can be used for microscale modulation of light intensity. The spatial distribution of the transmission intensity in the proposed intensity filter can also be manipulated by changing the polarization angle of the linearly polarized incident light, which has also been validated by the experimental results shown in **Figure 4c**. Moreover, because

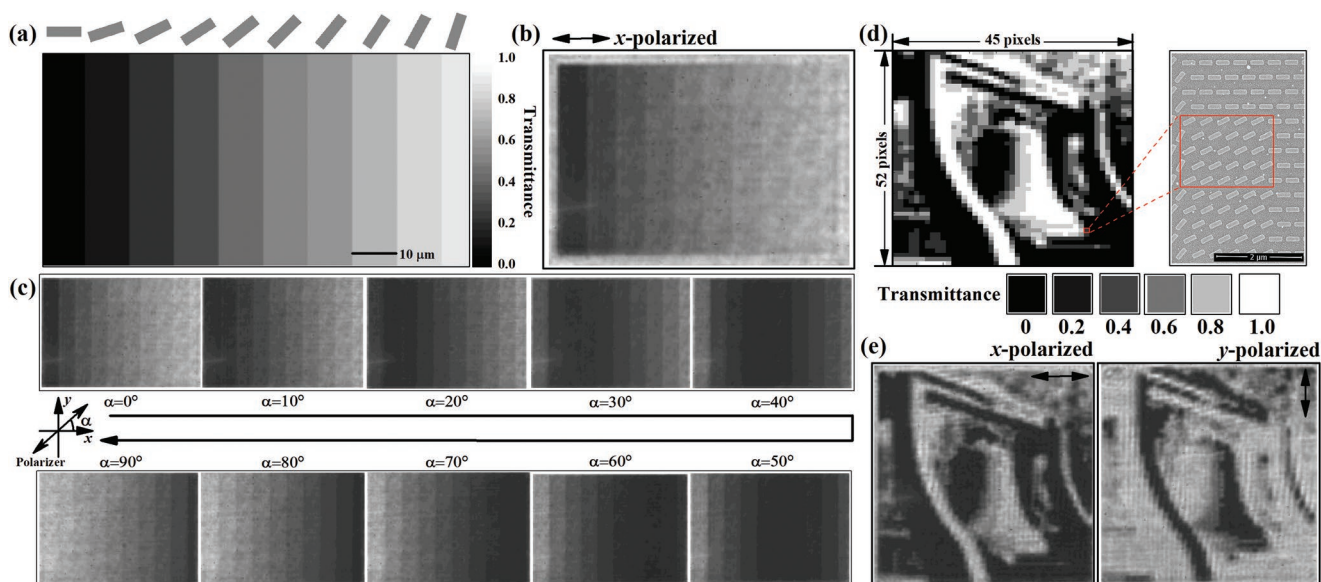


Figure 4. Manipulation of the transmission intensity on the microscale with the designed bilayer metasurface. a) A schematic of the designed gradient optical intensity filter and the corresponding calculated results for the transmission intensity distribution under x -polarized illumination (using Equation (4) while assuming A equals 1). The designed filter has ten separate regions in which $\sin^2\theta$ (where θ is the orientation angle of the nanorods) varies from 0 to 0.9 at a stepwise rate of 0.1. b) The experimental results of the transmission intensity distribution under x -polarized illumination at 1200 nm. c) The variation of the transmission intensity distribution under linearly polarized illumination with different polarization angles at 1200 nm. d) Schematic of the designed gray image (the school bell of Nankai University). The designed image has 45 pixels in the x -direction and 52 pixels in the y -direction, and each pixel consists of 5×5 unit cells of the bilayer metasurface with the same orientation angle θ . The bilayer nanorods constructing the image can be divided into six types in which the square value of the sine value of the orientation angle θ is equal to 0, 0.2, 0.4, 0.6, 0.8, and 1.0. e) The experimental results of the gray image under x and y -polarized illumination at 1200 nm.

the scale of the unit cell of the proposed bilayer metasurface is less than $1 \mu\text{m}$, the proposed design can be utilized to realize manipulation of the transmission intensity on the microscale. We further designed a gray image based on the proposed bilayer metasurface for experimental validation. The schematic for the designed gray image (the school bell of Nankai University) is shown in Figure 4d. The designed image has 45 pixels in the x -direction and 52 pixels in the y -direction, and each pixel consists of 5×5 unit cells of the bilayer metasurface with the same orientation angle θ (as shown in the inset SEM image). The transmission intensity of the designed gray image has six different values that are associated with six different orientation angles for the nanorods. The experimental results of the gray image under x and y -polarized incident light at 1200 nm are shown in Figure 4e. The gray image under x -polarized illumination is in good agreement with the designed image, while the intensity distribution is reversed for the y -polarized incident light. To obtain a good comparison between the designed image and the experimentally measured image, the size of the individual pixels in the gray image was designed to be $\approx 2 \mu\text{m} \times 1.7 \mu\text{m}$ (5×5 unit cells) with consideration for the resolution of our imaging system. Actually, the transmission intensity of each unit cell can be manipulated independently. The experimental results in Figure 4 validate that the proposed bilayer metasurface can be utilized to realize full manipulation of light intensity on the microscale, which can be widely used for microscale modulation of light intensity and gray imaging with high resolution.

The polarization-selective transmission in the proposed design also provides an alternative method for polarization-encoded imaging. To obtain polarization-encoded images with single

and dual outputs, we utilized bilayer metasurfaces composed of three different basic nanostructures: x -nanorods (orientation angle θ equals 0°), y -nanorods (orientation angle θ equals 90°), and cross-nanorods (a combination of the x and y -nanorods), as shown in Figure 5a. The simulated and experimental results of the transmittance of these three encoding units under x and y -polarized illumination are shown in Figure 5b–e. The experimental results are in good agreement with the simulated results. These results indicate that the bilayer metasurface composed of y -nanorods is transparent (the transmittance is equal to that of the substrate) under x -polarized illumination at ≈ 1200 nm, while there is almost no transmittance in the bilayer metasurfaces composed of x -nanorods and cross-nanorods. For y -polarized incident light, the bilayer metasurface composed of x -nanorods is transparent at ≈ 1200 nm, while there is almost no transmittance in the bilayer metasurfaces composed of the y -nanorods and cross-nanorods. Thus, we can treat the bilayer metasurface composed of y -nanorods as element “1” and the bilayer metasurfaces composed of x -nanorods and cross-nanorods as element “0” for x -polarized incident light. For y -polarized incident light, we can accordingly treat the bilayer metasurface composed of x -nanorods as element “1” and the bilayer metasurfaces composed of y -nanorods and cross-nanorods as element “0.” To validate this treatment visually, the experimental results for the imaging of periodic bilayer metasurfaces composed of the three different encoding units under x and y -polarized illumination are shown in Figure 5f. Schematics for the designed encoded images with both single (left design) and dual (right design) outputs are shown in Figure 5g. The inset of the SEM image shows the design details. The experimental results

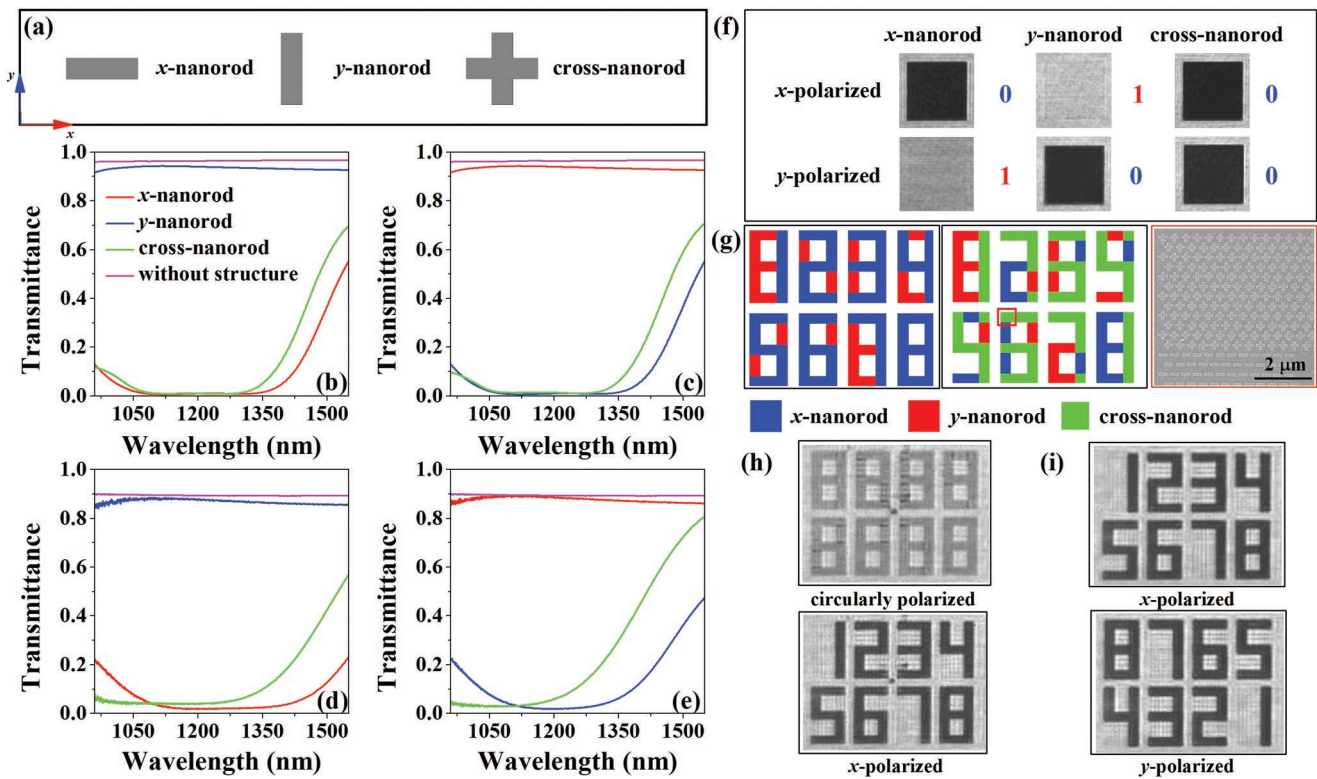


Figure 5. Optical polarization-encoded imaging with the designed bilayer metasurfaces. a) The designed encoding units: bilayer nanorods with the long axes along the x (x -nanorod) and y (y -nanorod) directions and bilayer cross-nanorods. b) Simulated and d) experimental results of the transmittance of the encoding units under x -polarized illumination. c) Simulated and e) experimental results of the transmittance of the encoding units under y -polarized illumination. f) Schematic for the optical polarization encoding. Inset: Captured images of the periodic bilayer metasurfaces composed of different encoding units under x and y -polarized illumination. g) Schematic of the designed optical polarization-encoded image composed of two and three coding units. The inset SEM image is taken from the area inside the red boundary. h) The experimental results for the polarization-encoded image composed of two coding units under circularly polarized and x -polarized illumination at 1200 nm. i) The experimental results of the polarization-encoded image composed of three coding units under x and y -polarized illumination at 1200 nm.

for polarization-encoded imaging with a single output are shown in Figure 5h. The designed image emerges under x -polarized incident light. It is worth mentioning that the transmittances of the bilayer metasurfaces composed of x and y -nanorods under illumination with natural light are the same, which will result in a natural hiding of the encoded image. This can be indirectly validated by the experimental results under circularly polarized incident light shown in Figure 5h. The experimental results of polarization-encoding imaging with dual outputs are shown in Figure 5i. Two independent images emerge under x and y -polarized incident light. We also investigated polarization-encoded imaging under linearly polarized illumination at different polarization angles (see Figure S5 in the Supporting Information). The results in Figure 5h,i are in good agreement with the designed results, which expands the applications of the proposed metasurface to include polarization-encoded imaging.

The proposed bilayer metasurface can also be used for optical anti-counterfeiting by utilizing the polarization conversion effect. Figure 6a,b shows the simulated results for t_{xx} and t_{yx} of the bilayer metasurfaces as a function of the orientation angle θ of the nanorods at 1100, 1200, and 1300 nm. The results indicate the existence of a polarization conversion effect ($t_{yx} \neq 0$) in the proposed bilayer metasurfaces when the

long axis of the nanorods is not along the x or y -axis. The polarization conversion effect in the bilayer metasurfaces is maximized when the orientation angle of the nanorods is equal to 45° . Based on this polarization conversion effect, we chose three bilayer metasurfaces composed of nanorods with orientation angles equal to 0° , 45° , and 90° to realize optical anti-counterfeiting by combining two quick response (QR) codes. A schematic of the designed counterfeit-proof QR code is shown in Figure 6c. The designed counterfeit-proof QR code has 41 pixels in the x -direction and 48 pixels in the y -direction, and each pixel consists of 5×5 unit cells of the bilayer metasurface with the same orientation angle θ . The designed counterfeit-proof QR code is a combination of QR code 1 (presenting information for the word “nankai”) and QR code 2 (presenting information for the word “metasurfaces”). The gray area in the counterfeit-proof QR code is identical to the white area in QR code 2, while the black and white area in the counterfeit-proof QR code is identical to the corresponding area in QR code 1. The experimental results of the counterfeit-proof QR code are shown in Figure 6d. When illuminated with natural light, the transmittances of the bilayer metasurfaces composed of nanorods with orientation angles equal to 0° , 45° , and 90° are the same, which results in a natural hiding

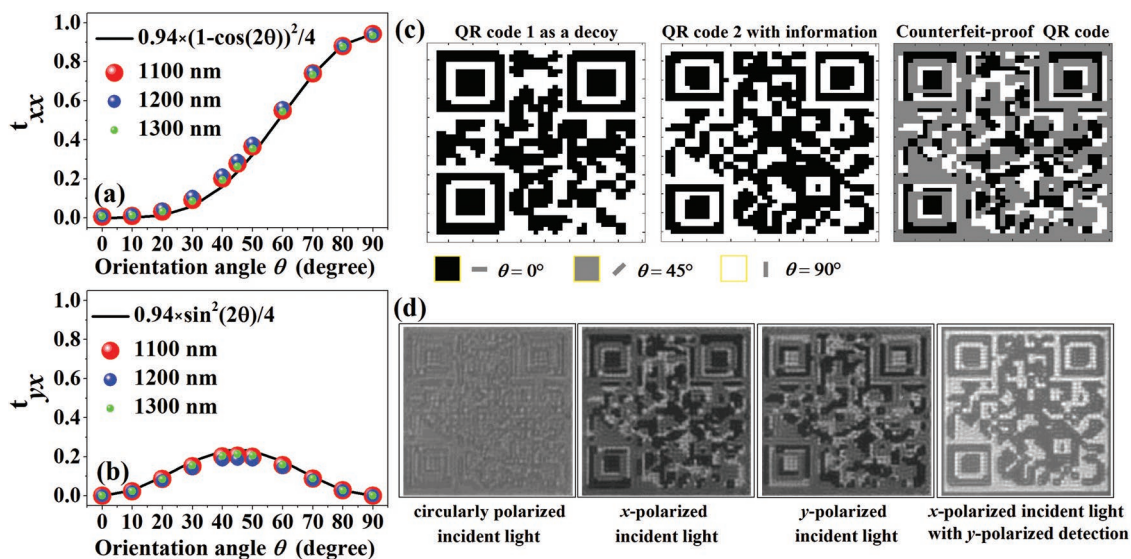


Figure 6. Optical anti-counterfeiting with the designed bilayer metasurfaces. The simulated results of the modular square $t_{ij} = |T_{ij}|^2$ of the transmission coefficients of the bilayer metasurfaces as a function of the orientation angle θ of the nanorods at 1100, 1200, and 1300 nm: a) t_{xx} and b) t_{yx} . The lines in (a) and (b) denote the $I_{xx} \propto (1 - \cos(2\theta))^2$ and $I_{yx} \propto \sin^2(2\theta)$ dependence, respectively. c) Schematic of the designed counterfeit-proof QR code. The designed QR code has 41 pixels in the x-direction and 48 pixels in the y-direction, and each pixel consists of 5×5 unit cells of the bilayer metasurface with the same orientation angle θ . The designed QR code consists of three types of bilayer metasurfaces in which the orientation angle θ of the nanorods is 0° , 45° , and 90° . d) The experimental results of the QR code under illumination with different polarization states at 1200 nm (the last image is obtained under x-polarized illumination with an analyzer along the y-axis).

of the encoded image. This can be indirectly validated by the experimental results under circularly polarized incident light. For x-polarized incident light, there is no transmittance in the area composed of nanorods with an orientation angle equal to 0° ; the area composed of nanorods with an orientation angle equal to 45° is semitransparent, while the area composed of nanorods with an orientation angle equal to 90° is transparent. For y-polarized incident light, the intensity distribution is reversed for the areas composed of nanorods with orientation angles equal to 0° and 90° . We also experimentally investigated the imaging of the counterfeit-proof QR code under linearly polarized illumination with different polarization angles (see Figure S6 in the Supporting Information). These results indicate that the information cannot be decrypted under natural light or polarized light. The information can only be decrypted under x or y-polarized incident light by adding an analyzer whose transmission axis is orthogonal to the polarization direction of the incident light. The results presented in Figure 6 and Figure S6 (Supporting Information) validate that the proposed bilayer metasurfaces can be utilized to realize optical anti-counterfeiting in the near-infrared band.

Ascribed to the broadband optical response of the proposed bilayer metasurfaces, all the mentioned applications are possible over a broad wavelength range. Figure 7 shows the experimental results of the designed devices for microscale modulation of light intensity, gray imaging with high resolution, optical polarization encoding, and anti-counterfeiting at different wavelengths. The results confirm that the optical functionalities of the designed devices remain constant over a broad wavelength range, which is quite beneficial for their practical application. The minute differences between the images in Figure 7d are attributed to the fabrication tolerances

of the bilayer metasurface composed of cross-nanorods, which can be verified by the experimental measurement results in Figure 5e.

In conclusion, we proposed the design specifications, simulated demonstrations, and experimental validations of bilayer metasurfaces for full and broadband transmission intensity manipulation of linearly polarized light in the near-infrared region. The realization of full and broadband transmission intensity manipulation of linearly polarized light is ascribed to the polarization-selective transmission in the proposed bilayer metasurfaces. The simulated results indicate that the proposed bilayer metasurfaces can be treated as a linear polarizer from 1050 to 1350 nm with a greater than 98% transmission ratio and a greater than 90% working efficiency. The experimental results are in good agreement with the simulated results. We also demonstrate that the optical response of the proposed bilayer metasurfaces is wide-angle and has a low requirement for the alignment of the two layers. Based on these results, we further demonstrate that the transmission intensity of linearly polarized light can be fully manipulated on the microscale by independently adjusting the orientation angle of each nanorod in the proposed bilayer metasurface. We experimentally validate that the proposed bilayer metasurfaces, which have the advantages of a compact design, a simple structure, having low cost, being alignment free, having broadband and wide-angle optical response, can be widely used for microscale modulation of light intensity, gray imaging with high resolution, optical polarization encoding, and anti-counterfeiting. Compared with well-known wire-grid polarizers, our approach can realize not only full and broadband polarization-selective transmission in the near-infrared region but also arbitrary and broadband transmission intensity manipulation of linearly polarized light on

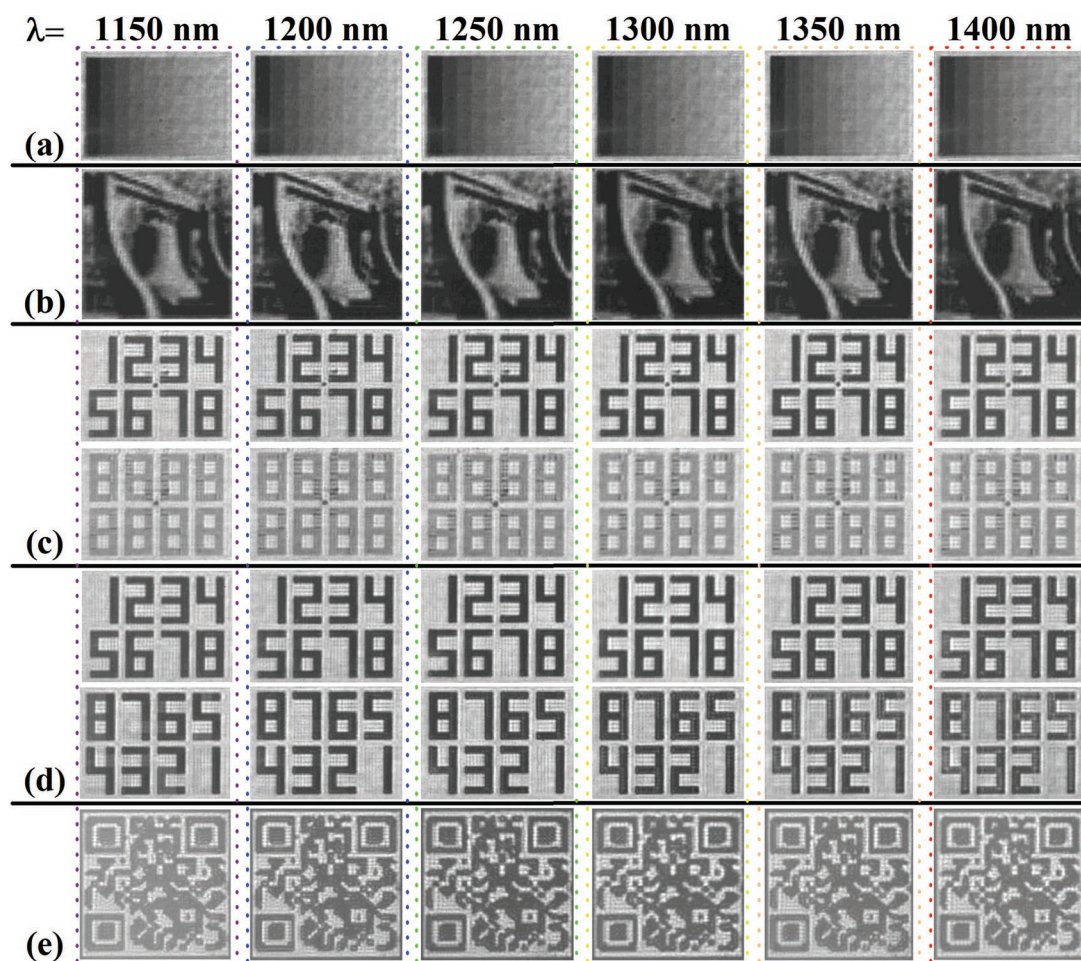


Figure 7. The performance of the designed bilayer metasurfaces at different wavelengths. a) The experimental results of the transmission intensity distribution in the designed gradient optical intensity filter (Figure 4a) under x-polarized illumination at different wavelengths. b) The experimental results of the designed gray image (Figure 4d) under x-polarized illumination at different wavelengths. c) The experimental results of the polarization-encoded image (Figure 5g) composed of two coding units under circularly and x-polarized illumination at different wavelengths. d) The experimental results of the polarization-encoded image (Figure 5i) composed of three coding units under x-polarized and y-polarized illumination at different wavelengths. e) The experimental results of the counterfeit-proof QR code (Figure 6c) with the analyzer along the y-axis (under x-polarized illumination at different wavelengths).

the microscale, which provides an effective means for the commercialization of few-layer metasurfaces for microscale light intensity manipulation.

Experimental Section

Sample Fabrication: The proposed bilayer metasurfaces were fabricated by electron-beam lithography (EBL) and Al lift-off processes (as shown in Figure S7 in the Supporting Information). A 200 nm thick ZEP520A positive electron-beam resist was initially spin-coated onto a microscope glass slide, and then the nanorod pattern was exposed using an EBL system (RAITH 150) at 30 keV. After exposure, the sample was developed in n-amyl acetate for 60 s, rinsed with isopropanol, and then blown dry using pure nitrogen. A 30 nm thick Al film was subsequently deposited by using an electron-beam evaporator (Temescal BJD-2000). After the resist was removed by means of a ZEP remover (ZDMAC), the first Al nanorod layer was created. A 130 nm thick layer of the SU-8 polymer was then spin-coated onto the sample and UV-cured. The second nanorod layer in Al was prepared by repeating the EBL and Al lift-off processes.

Finally, a 130 nm thick layer of the SU-8 polymer was spin-coated on top of the sample and UV-cured. Each of the eight completed metasurfaces was less than $100 \mu\text{m} \times 100 \mu\text{m}$ in size. In addition, the misalignment between the two layers of nanorods was less than 100 nm, which was verified by high-resolution SEM imaging of the top view of the fabricated sample (see Figure S8 in the Supporting Information).

Experimental Measurements: The transmission spectra were measured by using a Fourier transform infrared spectrometer (VERTEX 70). The spectral data were acquired with OPUS 6.0 software. Air was used as the reference for measuring the transmittance. The measurements of the images were based on a home-built microscope, as shown in Figure S9 in the Supporting Information. The light source was a supercontinuum laser (NKT SuperK EXR-20), and the laser beam was collimated with a fiber collimator. Then, the collimated beam was passed through an achromatic quarter-wave plate (B. Halle Nachfl) to generate a circularly polarized beam. Then, the collimated beam was passed through a broadband infrared polarizer (Sigma SPFN-30c-26). The collimated beam traveled through air onto the substrate of the metasurface. The output light from the sample was collected with an objective (Sigma NIR plan apo $50\times$, $\text{NA} = 0.67$), another broadband infrared polarizer (Sigma SPFN-30c-26), and an InGaAs camera (HAMAMATSU InGaAs C10633).

The images were obtained with the software for the InGaAs camera. The broadband infrared polarizer in the beam collection section was only used for the measurements of the QR code images.

Supporting Information

Supporting Information is available from the Wiley Online Library or from the author.

Acknowledgements

This work was supported by the National Key Research and Development Program of China (2016YFA0301102 and 2017YFA0303800), the National Natural Science Foundation of China (91856101, 11774186, and 11574163), the Natural Science Foundation of Tianjin for Distinguished Young Scientists (18JCQJC45700), the China Postdoctoral Science Foundation (2018M640224 and 2018M640229), the Natural Science Foundation of Tianjin (16CQNJC01700), and the 111 Project (B07013). The work was partly performed at the ACT node of the Australian National Fabrication Facility.

Conflict of Interest

The authors declare no conflict of interest.

Keywords

few-layer metasurfaces, integrated optical devices, light intensity manipulation, optical anti-counterfeiting, polarization-encoded imaging

Received: February 13, 2019

Revised: April 10, 2019

Published online: May 2, 2019

-
- [1] A. Kristensen, J. K. Yang, S. I. Bozhevolnyi, S. Link, P. Nordlander, N. J. Halas, N. A. Mortensen, *Nat. Rev. Mater.* **2017**, *2*, 16088.
 [2] F. Yue, C. Zhang, X. F. Zang, D. Wen, B. D. Gerardot, S. Zhang, X. Chen, *Light: Sci. Appl.* **2018**, *7*, 17129.
 [3] X. Duan, N. Liu, *ACS Nano* **2018**, *12*, 8817.
 [4] C. Zhang, D. Wen, F. Yue, Y. Intaravanne, W. Wang, X. Chen, *Phys. Rev. Appl.* **2018**, *10*, 034028.

- [5] Y. D. Shah, J. Grant, D. Hao, M. Kenney, V. Pusino, D. R. Cumming, *ACS Photonics* **2018**, *5*, 663.
 [6] Y. Ra'Di, C. R. Simovski, S. A. Tretyakov, *Phys. Rev. Appl.* **2015**, *3*, 037001.
 [7] V. S. Asadchy, I. A. Faniayeu, Y. Ra'Di, S. A. Khakhomov, I. V. Semchenko, S. A. Tretyakov, *Phys. Rev. X* **2015**, *5*, 031005.
 [8] P. C. Li, Y. Zhao, A. Alu, E. T. Yu, *Appl. Phys. Lett.* **2011**, *99*, 221106.
 [9] W. Junlin, Z. Binzhen, W. Xin, D. Junping, *Opt. Mater. Express* **2017**, *7*, 1656.
 [10] X. Duan, S. Chen, H. Cheng, Z. Li, J. Tian, *Opt. Lett.* **2013**, *38*, 483.
 [11] T. Ellenbogen, K. Seo, K. B. Crozier, *Nano Lett.* **2012**, *12*, 1026.
 [12] L. Duempelmann, A. Luu-Dinh, B. Gallinet, L. Novotny, *ACS Photonics* **2016**, *3*, 190.
 [13] E. Heydari, J. R. Sperling, S. L. Neale, A. W. Clark, *Adv. Funct. Mater.* **2017**, *27*, 1701866.
 [14] C. Pelzman, S. Y. Cho, *Appl. Phys. Lett.* **2015**, *106*, 251101.
 [15] B. Yang, W. Liu, Z. Li, H. Cheng, S. Chen, J. Tian, *Adv. Opt. Mater.* **2018**, *6*, 1701009.
 [16] H. Cheng, Z. Liu, S. Chen, J. Tian, *Adv. Mater.* **2015**, *27*, 5410.
 [17] N. K. Grady, J. E. Heyes, D. R. Chowdhury, Y. Zeng, M. T. Reiten, A. K. Azad, J. T. Antoinette, A. R. D. Diego, H.-T. Chen, *Science* **2013**, *340*, 1304.
 [18] Z. Li, S. Chen, C. Tang, W. Liu, H. Cheng, Z. Liu, J. Li, J. Tian, *Appl. Phys. Lett.* **2014**, *105*, 201103.
 [19] C. Zhang, C. Pfeiffer, T. Jang, V. Ray, M. Junda, P. Uprety, P. Nikolas, G. Anthony, L. J. Guo, *Laser Photonics Rev.* **2016**, *10*, 791.
 [20] Z. Li, W. Liu, H. Cheng, J. Liu, S. Chen, J. Tian, *Sci. Rep.* **2016**, *6*, 35485.
 [21] W. Luo, S. Sun, H. X. Xu, Q. He, L. Zhou, *Phys. Rev. Appl.* **2017**, *7*, 044033.
 [22] Z. Li, W. Liu, H. Cheng, S. Chen, J. Tian, *Sci. Rep.* **2017**, *7*, 8204.
 [23] M. Chen, E. Abdo-Sánchez, A. Epstein, G. V. Eleftheriades, *Phys. Rev. B* **2018**, *97*, 125433.
 [24] T. Cai, G. M. Wang, H. X. Xu, S. W. Tang, H. Li, J. G. Liang, Y. Q. Zhuang, *Ann. Phys. (Berlin)* **2018**, *530*, 1700321.
 [25] C. C. Chang, L. Huang, J. Nogan, H. T. Chen, *APL Photonics* **2018**, *3*, 051602.
 [26] C. Saeidi, D. van der Weide, *Appl. Phys. Lett.* **2013**, *103*, 183101.
 [27] L. Huang, C. C. Chang, B. Zeng, J. Nogan, S. N. Luo, A. J. Taylor, A. K. Azad, H.-T. Chen, *ACS Photonics* **2017**, *4*, 2111.
 [28] X. L. Hu, L. B. Sun, Q. J. Wu, L. S. Wang, S. A. Bai, Q. Li, S. M. Yang, R. Z. Tai, M. Mohr, H. J. Fecht, L. Q. Wang, D. X. Zhang, J. Z. Jiang, *J. Appl. Phys.* **2017**, *121*, 153105.
 [29] Y. Zhao, M. A. Belkin, A. Alù, *Nat. Commun.* **2012**, *3*, 870.
 [30] E. D. Palik, *Handbook of Optical Constants of Solids*, Academic Press, NY **1998**.